

# ELLIPTIC-SPLINE SOLUTIONS FOR LARGE LOCALIZATIONS IN A CIRCULAR BLATZ-KO CYLINDER DUE TO GEOMETRIC SOFTENING

HUI-HUI DAI\* AND XIAOCHUN PENG†

**Abstract.** It has been known that geometric softening can induce strain localizations in solids. However, it is very difficult to analytically capture the localized deformation states within a three-dimensional framework, especially when the deformation is large. In this paper, we introduce a novel approach, which resembles the use of a spline to approximate a curve, to construct analytical (asymptotic) solutions for large localizations in a circular cylinder composed of a Blatz-Ko material due to geometric softening. The asymptotic normal form equation (in the form of an ODE) valid for the axial stretch in a small neighborhood is first derived and then a set of these equations, each valid in a small neighborhood, can be obtained. The union of these small neighborhoods can cover a large range of the axial stretch and as a result this set of equations governs the deformation states for the axial stretch in a large interval. Through a phase-plane analysis on this set of ODEs we manage to obtain the analytical solutions (in the form of a spline of elliptic integrals) for the large strain localizations. Both a force-controlled problem and a displacement-controlled problem are solved and the analytical results capture well the non-uniqueness of the stress-displacement relation and the snap-through phenomenon, which are often observed in experiments when strain localizations happen. And, some insightful information on the bifurcation points, is obtained. The important geometric size effect is also discussed through the analytical solutions.

**Key words.** strain localization, post-bifurcation analysis, Blatz-Ko material

**AMS subject classifications.** 74B20, 74G10, 74G60, 35A20

**1. Introduction.** When a specimen under loading changes from a homogeneous deformation state to an inhomogeneous one with large strain(s) in a localized region, we say a strain localization happens. This is a widely spread phenomenon in solids (see Bower [11]). Strain localization may lead to the failure of a specimen, and a clear understanding of this phenomenon is thus important. In continuum mechanics, the loss of ellipticity caused by strain softening (in the true stress-strain curve some part has a negative slope) may lead to the onset of localized deformations. However, to capture the post-bifurcation localized states analytically (or even numerically) after the onset is a difficult task, especially in a two/three-dimensional setting. Most analytical works on localizations in literature are based on one-dimensional models; see Coleman [1], Coleman and Hodgdon [2], Dai and Bi [3], Triantafyllidis and Aifantis [4], Triantafyllidis and Bardenhagen [5]. In these models, typically some gradient terms are present. In the first three papers, the gradient terms are present due to the consideration of the transverse effects (taken into account in an ad hoc manner). In the last two papers, the gradient terms arise due to the consideration of the microscopic effects (see Aifantis and Serrin [6] and Aifantis [7]). While analytical results based on one-dimensional theories can provide some useful insightful information on localizations, high-dimensional effects, which are important as observed in some experiments, are missed out. Jansen and Shah [8] did experiments on concrete cylinders and the results described well the localization properties. They obtained the typical

---

\*Department of Mathematics and Liu Bie Ju Center for Mathematical Sciences, City University of Hong Kong, 83 Tat Chee Avenue, Kowloon Tong, Hong Kong (mahhdai@cityu.edu.hk). The research of this work was supported by a grant from the Research Grants Council of the HKSAR, China (Project No.: CityU 101009).

†Department of Mathematics, City University of Hong Kong, 83 Tat Chee Avenue, Kowloon Tong, Hong Kong (pxiaochun2@cityu.edu.hk).

stress-displacement behavior for different height-diameter ratios with normal strength and high strength from two test series. An interesting finding is that the post-peak response seems not only a material property but is dependent on the specimen geometry. They found that the post-peak response becomes steeper with increasing length (or equivalently, the length-radius ratio) of the specimen. In the experiment by Gopalaratnam and Shah [9], it was found that the tangent value in the ascending part of the stress-strain curves seems to be independent of the specimen size but in the post-peak part there is a softening region and no unique stress-strain relation. These experiments indicate the importance of the high-dimensional effects. One may numerically compute localized deformations in a two/three-dimensional setting (see Tvergaard et al. [10]), but some undesirable dependence on selected mesh size and orientation could arise. Thus, it would be desirable if the localized solutions could be captured analytically in a two/three-dimensional setting.

Besides strain softening, if the nominal stress-strain curve has a local maximum due to geometric softening, strain localization can also happen (see Bower [11]). Geometric softening means that the specimen under test tends to soften as a result of the change in its cross sectional area. For example, consider the uniaxial extension test of a bar. The true stress-strain curve may be monotone increasing but the nominal/engineering stress-strain curve may have a local maximum due to the cross sectional area change and then the slope becomes negative (softening). After this maximum point, localized modes can appear and the deformation becomes inhomogeneous. But, as mentioned in Bower [11], “It is usually exceedingly difficult to compute what happens after localization”. Although strain localization due to geometric softening often happens for ductile (plastic) materials, it can also happen for nonlinearly elastic materials. Actually, Beatty [12] noticed that there is a local maximum in the nominal stress-strain curve due to geometric softening for a Blatz-Ko material (see Figure 2.2). Although it appears that no experimental observation of strain localization in this material has been reported, such a local maximum noticed by Betty indicates it can happen in a Blatz-Ko cylinder under tension/extension. Therefore, theoretically it will be interesting to capture the localized solutions to gain insights into this phenomenon (such as the bifurcation points in a force-controlled problem and a displacement-controlled problem, which may not be captured by a linearized theory; see the remark below (6.11) and that above (8.2)). In this paper, within a three-dimensional framework we shall construct analytical (asymptotic) solutions for large localized deformations in a circular Blatz-Ko cylinder due to geometric softening.

To deduce the analytical solutions for localizations in a three-dimensional setting, one needs to deal with coupled nonlinear partial differential equations (PDEs) together with complicated boundary conditions. Further, the existence of multiple solutions (corresponding to non-unique stress-strain relation) makes the problem even harder to solve. Within the framework of weak nonlinearity, sometimes the multiple scale method may be used to construct the post-bifurcation solutions in nonlinear elasticity. For example, Fu [13] used such a method to study the necking of an infinitely-long elastic plate. Recently, a method of coupled series-asymptotic expansions, which was first introduced to study nonlinear elastic waves (see [14, 15]), was adopted to tackle the solution bifurcations in thin/slender structures composed of nonlinearly elastic materials (see [16, 17, 18]). In particular, by such a methodology, Dai et al. [19] studied localizations in a slender cylinder composed of an *incompressible* hyperelastic material subjected to axial tension. Although the analytical results obtained in [19] can successfully capture some key experimental features, the analysis was carried

FIG. 2.1. *The geometry of the object of study.*

out within the framework of weak nonlinearity (small strains). More specifically, the asymptotic expansions of the stresses were at the deformation gradient  $\mathbf{F} = \mathbf{I}$ . Thus, the results obtained in that paper is only valid for small localizations near the initial undeformed state. For a Blatz-Ko material (a *compressible* hyperelastic material), the onset of localizations happens at a large axial strain value and also the axial strain can vary in a large interval (i.e., these are large localizations). In particular, the latter makes the assumption of weak nonlinearity invalid, and one has to do the analysis within the framework of strong nonlinearity. This causes a major difficulty to construct solutions from the original field equations. A main contribution of this paper is that we introduce a novel approach to overcome this difficulty.

This approach shares some similarity with using a spline to approximate a curve in a large variable interval through polynomials in many small neighborhoods with smoothness requirements at the joint points. Here, to construct the localization solutions with the axial strain/stretch value in a large interval, we first use the method of coupled series-asymptotic expansions to derive the asymptotic normal form equation (ANFE) valid in a small neighborhood of an axial stretch value. Then, by taking different values and the proper neighborhoods, we have a set of ANFEs. By imposing the smoothness requirements at joint points, these equations can give the localization solutions valid in a large stretch interval. Since the solution of each ANFE can be represented by elliptic integral(s), we call the analytical solutions for large localizations constructed by the present approach to be the elliptic-spline solutions.

The rest of the paper is organized as follows. In section 2, we introduce the three-dimensional field equations for a Blatz-Ko material and the traction-free boundary conditions. Some results on the uniaxial tension are recalled. In section 3, by non-dimensionalization we extract the important small variable and two small parameters which characterize this problem. Then, in section 4 we derive the ANFE valid for the stretch value in a small neighborhood through the method of coupled series-asymptotic expansions. We show that the Euler-Lagrange equation can also lead to the same equation in section 5. The analytical solutions for localizations at near-critical loads are constructed in section 6. In section 7, by using the idea described above we derive the elliptic-spline solutions for large localizations for given engineering stress values. In section 8, we further manage to deduce solutions for a displacement-controlled problem. We also examine the strong ellipticity condition for the solutions obtained, and the smallest energy criterion is used to determine the preferred solutions. Based on the analytical solutions, we give some analysis on the geometrical size effect. Finally, some conclusions are drawn.

**2. Field equations and the uniaxial tension.** We study the axisymmetric deformations of a slender elastic circular cylinder subjected to axial forces at two ends, as shown in Figure 2.1. Suppose that the radius of the cylinder is  $a$  and the length is  $l$ . We shall use the cylindrical polar coordinate system and denote  $(R, \Theta, Z)$  and  $(r, \theta, z)$  the coordinates of a material point in the reference and current configurations, respectively.

We suppose that the cylinder is composed of a Blatz-Ko material, which is a kind

of compressible isotropic material. The strain energy function  $\Phi$  for this material is

$$\Phi = \frac{\mu}{2} \left( \frac{I_2}{I_3} + 2I_3^{1/2} - 5 \right), \quad (2.1)$$

where  $I_1, I_2, I_3$  are the principal invariants of the left Cauchy-Green deformation tensor  $\mathbf{B} = \mathbf{F}\mathbf{F}^T$  ( $\mathbf{F}$  is the deformation gradient). Such a material was first proposed by Blatz and Ko [20] as a model for foam rubber compressible materials undergoing large deformations. Moreover the nominal stress tensor  $\Sigma$  is given by

$$\Sigma = \frac{\partial \Phi}{\partial \mathbf{F}^T}, \quad \Sigma_{Ai} = \frac{\partial \Phi}{\partial F_{iA}}, \quad (2.2)$$

where  $i = 1, 2, 3$  corresponding to  $r, \theta$  and  $z$ , and  $A = 1, 2, 3$  corresponding to  $R, \Theta$  and  $Z$  respectively.  $\Sigma$  satisfies the field equations:

$$\frac{\partial \Sigma_{Rz}}{\partial R} + \frac{\partial \Sigma_{Zz}}{\partial Z} + \frac{\Sigma_{Rz}}{R} = 0, \quad \frac{\partial \Sigma_{Rr}}{\partial R} + \frac{\partial \Sigma_{Zr}}{\partial Z} + \frac{\Sigma_{Rr} - \Sigma_{\Theta\theta}}{R} = 0. \quad (2.3)$$

We consider the case that the lateral surface of the cylinder is traction-free. Thus, we have the following boundary conditions:

$$\Sigma_{Rr}|_{R=a} = 0, \quad \Sigma_{Rz}|_{R=a} = 0. \quad (2.4)$$

Equations (2.3) together with (2.4) provide the governing equations for two unknowns  $r$  and  $z$ . They are coupled nonlinear PDEs with complicated boundary conditions. And as far as we know, there is no analytical method available to solve them for general end conditions.

For the homogenous deformation induced by uniaxial tension, it is possible to get the analytical solution, which was given in Beatty [12]. In this case, we have

$$r(R, Z) = \delta_1 R, \quad z(R, Z) = \delta_2 Z, \quad (2.5)$$

where  $\delta_1$  and  $\delta_2$  are constants, corresponding to the radial and axial stretches respectively. In this case the field equations (2.3) are naturally satisfied. From (2.4)<sub>1</sub>, we have  $\delta_1 = \delta_2^{-1/4}$ . Then the axial engineering (nominal) stress  $\gamma$  and Cauchy stress  $\gamma_C$  can be expressed by the axial stretch  $\delta_2$  (see Beatty [12]):

$$\gamma = \delta_2^{-1/2} - \delta_2^{-3}, \quad \gamma_C = 1 - \delta_2^{-5/2}. \quad (2.6)$$

Here  $\mu$  has been taken to be 1. Plots of the engineering and Cauchy stresses have been provided in Beatty [12]. Here we replot them in Figure 2.2, from which we see that the Cauchy stress is monotone increasing but due to geometric softening the engineering stress has a local maximum at  $\delta_2^* = 2.04767$ . After  $\delta_2 > \delta_2^*$ , the deformation becomes inhomogeneous and a localization can appear.

To study localizations induced by geometric softening, we first consider a small disturbance superimposed on the prestretched state of the cylinder. In this case, the coordinates of a material point in the current configuration can be expressed as

$$r(R, Z) = \delta_1 R + U(R, Z), \quad z(R, Z) = \delta_2 Z + W(R, Z), \quad (2.7)$$

where  $U(R, Z)$  and  $W(R, Z)$  are two small disturbance functions. Then the corresponding deformation gradient tensor  $\mathbf{F}$  in matrix form is given by

$$F_{iA} = (\delta_{ij} + \eta_{ij}) \bar{F}_{jA}, \quad (2.8)$$

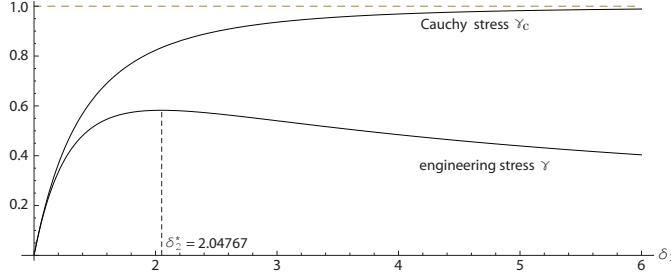


FIG. 2.2. *Cauchy and engineering stress-stretch relations for the Blatz-Ko cylinder in a homogeneous uniaxial tension.*

where

$$\bar{\mathbf{F}} = \begin{pmatrix} \delta_1 & 0 & 0 \\ 0 & \delta_1 & 0 \\ 0 & 0 & \delta_2 \end{pmatrix}, \quad \boldsymbol{\eta} = \begin{pmatrix} \frac{U_{\bar{F}}}{\delta_1} & 0 & \frac{U_Z}{\delta_2} \\ 0 & \frac{U}{R\delta_1} & 0 \\ \frac{W_{\bar{F}}}{\delta_1} & 0 & \frac{W_Z}{\delta_2} \end{pmatrix}. \quad (2.9)$$

It is convenient to introduce a tensor function with components  $\kappa_{ij}$  through  $\kappa_{ij} = \bar{F}_{iA}\Sigma_{Aj}$ . Since the deformation superimposed on the prestretched configuration is small, i.e.  $|\boldsymbol{\eta}| = \max_{1 \leq i, j \leq 3} |\eta_{ij}| \ll 1$ ,  $\kappa_{ij}$  can be expanded at the finite deformation gradient  $\bar{\mathbf{F}}$  up to any order. The formula containing terms up to the third-order material nonlinearity has been provided in Fu & Ogden [21], which is given as

$$\kappa_{ji} = \mathcal{A}_{ji}^0 + \mathcal{A}_{jilk}^1 \eta_{kl} + \frac{1}{2} \mathcal{A}_{jilknm}^2 \eta_{kl} \eta_{mn} + \frac{1}{6} \mathcal{A}_{jilknmqp}^3 \eta_{kl} \eta_{mn} \eta_{pq} + o(|\boldsymbol{\eta}|^4), \quad (2.10)$$

where  $\bar{J}^{-1}\mathcal{A}^0$ ,  $\bar{J}^{-1}\mathcal{A}^1$ ,  $\bar{J}^{-1}\mathcal{A}^2$  and  $\bar{J}^{-1}\mathcal{A}^3$  are the tensors of instantaneous elastic moduli defined by

$$\begin{aligned} \bar{J} &= \det \bar{\mathbf{F}}, \quad \mathcal{A}_{ji}^0 = \bar{F}_{jA} \frac{\partial \Phi}{\partial F_{iA}} \Big|_{\mathbf{F}=\bar{\mathbf{F}}}, \quad \mathcal{A}_{jilk}^1 = \bar{F}_{jA} \bar{F}_{lB} \frac{\partial^2 \Phi}{\partial F_{iA} \partial F_{kB}} \Big|_{\mathbf{F}=\bar{\mathbf{F}}}, \\ \mathcal{A}_{jilknm}^2 &= \bar{F}_{jA} \bar{F}_{lB} \bar{F}_{nC} \frac{\partial^3 \Phi}{\partial F_{iA} \partial F_{kB} \partial F_{mC}} \Big|_{\mathbf{F}=\bar{\mathbf{F}}}, \\ \mathcal{A}_{jilknmqp}^3 &= \bar{F}_{jA} \bar{F}_{lB} \bar{F}_{nC} \bar{F}_{qD} \frac{\partial^4 \Phi}{\partial F_{iA} \partial F_{kB} \partial F_{mC} \partial F_{pD}} \Big|_{\mathbf{F}=\bar{\mathbf{F}}}. \end{aligned} \quad (2.11)$$

From (2.1) and  $\delta_1 = \delta_2^{-1/4}$  one can see that the components of these moduli can be expressed in terms of  $\delta_2$ . Then from (2.9) and  $\kappa_{ij} = \bar{F}_{iA}\Sigma_{Aj}$  we can obtain the expansions of  $\Sigma_{Ai}$ . Finally, substituting them into (2.3-2.4) we can obtain two complicated PDEs together with two complicated boundary conditions for two unknowns  $U$  and  $W$ . It is extremely difficult (if possible) to analytically solve such a nonlinear problem directly. Here, we shall adopt the coupled series-asymptotic expansion method developed in Dai & Huo [14], Dai & Fan [15] and Dai & Cai [16] to tackle this problem. Firstly, we shall nondimensionalize this system to identify the relevant small variable and small parameters.

**3. Non-dimensionalized equations.** The first step is to introduce a very important transformation (cf. Dai & Huo [14])

$$U = u\delta_1 R, \quad s = \delta_1^2 R^2. \quad (3.1)$$

Here, scaling  $U$  by  $\delta_1 R$  is suggested by (2.7)<sub>1</sub> and introducing  $s$  is for the purpose to eliminate  $1/R$  in (2.3). The length of the cylinder in the prestretched state is  $\delta_2 l$ ,

which is a natural choice to scale the spatial variables. Suppose that we consider the elongation up to  $h$  with the constraint  $\epsilon = \frac{h}{\delta_2 l}$  being small ( $h$  is a measure of the axial displacement). Thus, we introduce the dimensionless quantities through the following scales:

$$s = \delta_2^2 l^2 \tilde{s}, \quad Z = \delta_2 l \tilde{z}, \quad W = h \tilde{w}, \quad u = \frac{h}{\delta_2 l} \tilde{u}. \quad (3.2)$$

In the prestretched state the radius becomes  $\delta_1 a$ . We consider the case that the square of the radius-length ratio is small, i.e.  $\nu = (\frac{\delta_1 a}{\delta_2 l})^2$  is a small parameter. It should be noted that even if  $a/l$  is relatively large,  $\nu$  can still be small (since  $\delta_1^2/\delta_2^2$  could be small).

Substituting (3.1) and (3.2) into Eqs. (2.3), we obtain

$$3\delta_2^{-1} w_{zz} + 4\delta_2 w_s + 2(1 + \delta_2^{\frac{5}{2}})u_z + 2s[2\delta_2 w_{ss} + (1 + \delta_2^{\frac{5}{2}})u_{sz}] + \dots = 0, \quad (3.3)$$

$$24\delta_2^{\frac{7}{2}} u_s + 2(1 + \delta_2^{\frac{5}{2}})w_{sz} + \delta_2^{\frac{3}{2}} u_{zz} + 12\delta_2^{\frac{7}{2}} s u_{ss} + \dots = 0. \quad (3.4)$$

Here and hereafter, we have dropped the tilde for convenience. The full forms of (3.3) and (3.4) are very lengthy and are omitted for brevity. Substituting (3.1) and (3.2) into the traction-free boundary conditions (2.4), we obtain

$$4\delta_2^{\frac{11}{4}} u + \delta_2^{\frac{7}{4}} w_z + 6\delta_2^{\frac{11}{4}} s u_s + \epsilon[\delta_2^{\frac{7}{4}} u w_z - 6\delta_2^{\frac{11}{4}} u^2 + s(-4\delta_2^{\frac{1}{4}} w_s^2 - \delta_2^{\frac{3}{4}} u_z^2 - 24\delta_2^{\frac{11}{4}} u u_s - (2\delta_2^{-\frac{3}{4}} + 6\delta_2^{\frac{7}{4}})u_z w_s) - 24\delta_2^{\frac{11}{4}} s^2 u_s^2] + \dots = 0, \quad \text{at } s = \nu, \quad (3.5)$$

$$2\delta_2^{\frac{1}{4}} w_s + \delta_2^{-\frac{3}{4}} u_z + \epsilon[-4\delta_2^{\frac{1}{4}} u w_s - (\delta_2^{-\frac{3}{4}} + 4\delta_2^{\frac{7}{4}})u u_z - 4\delta_2^{-\frac{3}{4}} w_s w_z - (3\delta_2^{-\frac{7}{4}} + \delta_2^{\frac{3}{4}})u_z w_z - s(8\delta_2^{\frac{1}{4}} u_s w_s + (2\delta_2^{-\frac{3}{4}} + 6\delta_2^{\frac{7}{4}})u_s u_z)] + \dots = 0, \quad \text{at } s = \nu \quad (3.6)$$

Equations (3.3)-(3.6) compose a new system that is still very complicated and difficult to be analyzed directly. However, it is characterized by a small variable  $s$  and two small parameters  $\epsilon$  and  $\nu$ , which permit us to use expansion methods to do simplifications.

**4. Coupled Series-Asymptotic Expansions.** Note that  $s$  is a small variable as  $0 \leq s \leq \nu$ . It can be seen that the two unknowns  $w$  and  $u$  of the system (3.3)-(3.6) depend on the variable  $z$ , the small variable  $s$  and the small parameter  $\epsilon$  and  $\nu$ , that is  $w = w(z, s; \epsilon, \nu)$ ,  $u = u(z, s; \epsilon, \nu)$ . As long as we assume that  $w$  and  $u$  are sufficiently smooth in  $s$ , they have series expansions in terms of the small variable  $s$ :

$$u(z, s; \epsilon, \nu) = u_0(z; \epsilon, \nu) + s u_1(z; \epsilon, \nu) + s^2 u_2(z; \epsilon, \nu) + \dots, \quad (4.1)$$

$$w(z, s; \epsilon, \nu) = w_0(z; \epsilon, \nu) + s w_1(z; \epsilon, \nu) + s^2 w_2(z; \epsilon, \nu) + \dots. \quad (4.2)$$

Substituting (4.1) and (4.2) into the traction-free boundary conditions (3.5) and (3.6), we obtain

$$4\delta_2^{\frac{11}{4}} u_0 + \delta_2^{\frac{7}{4}} w_{0z} + \nu(\delta_2^{\frac{7}{4}} w_{1z} + 10\delta_2^{\frac{11}{4}} u_1) + \epsilon(\delta_2^{\frac{7}{4}} u_0 w_{0z} - 6\delta_2^{\frac{11}{4}} u_0^2) + 10\delta_2^{\frac{11}{4}} \epsilon^2 u_0^3 + O(\nu^2, \epsilon\nu, \epsilon^3) = 0, \quad (4.3)$$

$$\begin{aligned}
& 2\delta_2^{\frac{1}{4}}w_1 + \delta_2^{-\frac{3}{4}}u_{0z} + \nu(\delta_2^{-\frac{3}{4}}u_{1z} + 4\delta_2^{\frac{1}{4}}w_2) - \epsilon[4\delta_2^{-\frac{3}{4}}w_1w_{0z} + (3\delta_2^{-\frac{7}{4}} + \delta_2^{\frac{3}{4}})u_{0z}w_{0z} + \\
& 4\delta_2^{\frac{1}{4}}u_0w_1 + (\delta_2^{-\frac{3}{4}} + 4\delta_2^{\frac{7}{4}})u_0u_{0z}] + \epsilon^2[6\delta_2^{-\frac{7}{4}}w_1w_{0z}^2 + (6\delta_2^{-\frac{11}{4}} + \delta_2^{-\frac{1}{4}})u_{0z}w_{0z}^2 + 6\delta_2^{\frac{1}{4}}u_0^2w_1 \\
& + (\delta_2^{-\frac{3}{4}} + 6\delta_2^{\frac{7}{4}})u_0^2u_{0z} + 8\delta_2^{-\frac{3}{4}}u_0w_1w_{0z} + (3\delta_2^{-\frac{7}{4}} + 3\delta_2^{\frac{3}{4}})u_0u_{0z}w_{0z}] + O(\nu^2, \epsilon\nu, \epsilon^3) = 0.
\end{aligned} \tag{4.4}$$

By neglecting  $O(\nu^2, \epsilon\nu, \epsilon^3)$ -terms, the above two equations contain five unknowns:  $w_0, w_1, w_2, u_0$  and  $u_1$  (other unknowns appear in  $O(\nu^2, \epsilon\nu)$ -terms). Thus, to form a closed-system, we need to find another three equations which contain and only contain these five unknowns. For this purpose we further substitute (4.1) and (4.2) into (3.3). The left hand becomes a series in  $s$  and all the coefficients of  $s^n$  ( $n = 0, 1, 2, \dots$ ) should vanish. As a result, we have an infinite system of equations with infinitely-many unknowns. However, it turns out that the two equations from the coefficients of  $s^0$  and  $s^1$  only contain the five unknowns appeared in (4.3) and (4.4)! These two equations are

$$\begin{aligned}
& [4\delta_2 - 8\epsilon w_{0z} + \epsilon^2(12\delta_2^{-1}w_{0z}^2 + 16u_0w_{0z})]w_1 + 2(1 + \delta_2^{\frac{5}{2}})u_{0z} \\
& + 3\delta_2^{-1}w_{0zz} + \epsilon\mathcal{L}_1(w_0, u_0) + \epsilon^2\mathcal{L}_2(w_0, u_0) = 0,
\end{aligned} \tag{4.5}$$

$$\begin{aligned}
& [16\delta_2 - \epsilon(32w_{0z} + 32\delta_2u_0) + \epsilon^2(48\delta_2^{-1}w_{0z}^2 + 48\delta_2u_0^2 + 64u_0w_{0z})]w_2 + \\
& 4(1 + \delta_2^{\frac{5}{2}})u_{1z} + 3\delta_2^{-1}w_{1zz} + \epsilon\mathcal{L}_3(w_0, w_1, u_0, u_1) + \epsilon^2\mathcal{L}_4(w_0, w_1, u_0, u_1) = 0,
\end{aligned} \tag{4.6}$$

where  $\mathcal{L}_i$  ( $i = 1, 2, 3, 4$ ) are operators on the arguments whose long expressions are omitted. Similarly, we substitute equations (4.1) and (4.2) into (3.4). It turns out the equation from the coefficient of  $s^0$  only contains the above-mentioned five unknowns! This equation is

$$\begin{aligned}
& [24\delta_2^{\frac{7}{2}} + 96\epsilon\delta_2^{\frac{7}{2}}u_0 + 240\epsilon^2\delta_2^{\frac{7}{2}}u_0^2]u_1 + 2(1 + \delta_2^{\frac{5}{2}})w_{1z} + \delta_2^{\frac{3}{2}}u_{0zz} \\
& + \epsilon\mathcal{L}_5(w_0, w_1, u_0) + \epsilon^2\mathcal{L}_6(w_0, w_1, u_0) = 0.
\end{aligned} \tag{4.7}$$

Equations (4.3)-(4.7) provide a closed nonlinear ODE system for the five unknowns. Mathematically, it is still very difficult to solve them directly. To go further, we shall use the smallness of the parameter  $\epsilon$ . From (4.5), we see that it is a linear algebraic equation for  $w_1$  if  $w_0$  and  $u_0$  are regarded to be known variables. Thus we can express  $w_1$  by  $w_0$  and  $u_0$ . This is another key why the present methodology works! Substituting  $w_1$  into (4.7), we can also express  $u_1$  by  $w_0$  and  $u_0$ . Similarly, we substitute  $w_1$  and  $u_1$  into (4.6) to obtain the expression of  $w_2$  in terms of  $w_0$  and  $u_0$ . We point out that in the process of obtaining expressions of  $w_1, u_1$  and  $w_2$  we drop  $O(\epsilon^3)$ -terms, to be consistent with (4.3) and (4.4). Finally, substituting  $w_1, u_1$  and  $w_2$  into (4.3) and (4.4) and omitting  $O(\nu^2, \epsilon\nu, \epsilon^3)$ -terms (to be consistent with (4.3) and (4.4)) yield two equations with only two unknowns  $w_0$  and  $u_0$ . It turns out that one equation can be integrated once, and as a result we obtain

$$\begin{aligned}
& 4\delta_2^{\frac{11}{4}}u_0 + \delta_2^{\frac{7}{4}}w_{0z} - \nu[(-\frac{5}{8}\delta_2^{-\frac{11}{4}} + \frac{1}{8}\delta_2^{-\frac{1}{4}})w_{0zzz} + (-\frac{5}{12}\delta_2^{-\frac{7}{4}} + \frac{1}{12}\delta_2^{\frac{3}{4}} + \frac{1}{12}\delta_2^{\frac{13}{4}})u_{0zz}] \\
& + \epsilon(\delta_2^{\frac{7}{4}}u_0w_{0z} - 6\delta_2^{\frac{11}{4}}u_0^2) + 10\epsilon^2\delta_2^{\frac{11}{4}}u_0^3 = 0,
\end{aligned} \tag{4.8}$$

and

$$\begin{aligned}
& -\delta_2^{\frac{7}{4}}u_0 - \frac{3}{2}\delta_2^{-\frac{7}{4}}w_{0_z} + \nu\left[\left(\frac{1}{2}\delta_2^{-\frac{15}{4}} - \frac{1}{16}\delta_2^{-\frac{5}{4}}\right)w_{0_{zzz}} + \left(\frac{1}{3}\delta_2^{-\frac{11}{4}} + \frac{1}{3}\delta_2^{-\frac{1}{4}} - \frac{1}{24}\delta_2^{\frac{9}{4}}\right)u_{0_{zz}}\right] \\
& + \epsilon\left(3\delta_2^{-\frac{11}{4}}w_{0_z}^2 - \frac{1}{2}\delta_2^{\frac{7}{4}}u_0^2\right) - 5\epsilon^2\delta_2^{-\frac{15}{4}}w_{0_z}^3 = C,
\end{aligned} \tag{4.9}$$

where  $C$  is an integration constant. Combining (4.8) and (4.9) by eliminating  $u_{0_{zz}}$ , we can obtain a cubic algebraic equation for  $u_0$ . Solving it by a perturbation method we can express  $u_0$  by  $w_0$  and the constant  $C$ . Then substituting this expression into (4.8) and using the perturbation method again, we obtain the following equation for the axial strain  $w_{0_z}$ :

$$\epsilon w_{0_z} + \epsilon^2 D_2 w_{0_z}^2 + \epsilon^3 D_3 w_{0_z}^3 + \epsilon \nu D_1 w_{0_{zzz}} = C_1, \tag{4.10}$$

where  $C_1$  is a constant, and

$$D_1 = \frac{-15 + 58\delta_2^{5/2} - 14\delta_2^5 + \delta_2^{15/2}}{24\delta_2^{9/2}(-6 + \delta_2^{5/2})}, \quad D_2 = -\frac{3(-16 + \delta_2^{5/2})}{4\delta_2(-6 + \delta_2^{5/2})}, \quad D_3 = \frac{5(-32 + \delta_2^{5/2})}{8\delta_2^2(-6 + \delta_2^{5/2})}. \tag{4.11}$$

The physical meaning of  $C_1$  can be identified. By considering the resultant force  $T$  acting on the material cross-section, after some calculations, we find  $C_1 = T/\pi a^2 E_T - D_0/E_T$ , where  $D_0 = -\delta_2^{-3} + \delta_2^{-1/2}$  is the engineering stress at  $\bar{\mathbf{F}}$  (i.e. the prestress) and  $E_T = 3\delta_2^{-4} - \frac{1}{2}\delta_2^{-3/2}$  is the tangent modulus at  $\bar{\mathbf{F}}$ .

If we retain the original dimensional variable and let  $V = W_{0_z} = \epsilon w_{0_z}$ , then we have

$$V + D_2 V^2 + D_3 V^3 + a^2 \delta_2^{-1/2} D_1 V_{ZZ} = \frac{\gamma - D_0}{E_T}, \tag{4.12}$$

where  $\gamma = T/\pi a^2$  is the engineering stress. We call (4.12) the asymptotic normal form equation (ANFE) of the field equations (2.3) together with the nonlinear boundary conditions (2.4). We point out that this equation was derived for small deformations superimposed on a prestretched state (see (2.9)) without an explicit restriction on  $\gamma$ .

**Remark:** For a fixed  $\delta_2$ , if we make a special choice  $\gamma = D_0$ , Eq. (4.12) then reduces to

$$-a^2 \delta_2^{-1/2} V_{ZZ} = D_1^{-1} V + D_1^{-1} D_2 V^2 + D_1^{-1} D_3 V^3, \tag{4.13}$$

which governs the variation of any possible bifurcated solution. The solution of this equation changes character when  $D_1^{-1} = 0$ , i.e.  $\delta_2 = \delta_2^* = 6^{2/5} = 2.04767$ . This may indicate a bifurcation takes place at  $\gamma = D_0|_{\delta_2^*} = 0.5824$  (which is the load maximum; cf. Figure 2.2). However, the critical load for bifurcation depends on the radius-length ratio (see the remark below (6.11)). When this ratio tends to zero (corresponding to an infinitely-long cylinder), the critical load coincides with the load maximum.

**5. The Euler-Lagrange equation.** Now, we shall derive the same equation from the variational principle by considering the energy.

We first expand the strain-energy function  $\Phi$  about the finitely deformed state  $\bar{\mathbf{F}}$  up to the fourth-order nonlinearity. Using the expressions obtained in the previous sections,  $\Phi$  can be represented in terms of  $w_0$ . Then, we find that the average stored energy over a cross section is given by

$$\begin{aligned}
\bar{\Psi} &= \frac{1}{\pi a^2} \int_0^a \int_0^{2\pi} \Phi R dR d\Theta \\
&= \Phi(\bar{\mathbf{F}}) + E_T \left( \frac{D_0}{E_T} V + \frac{1}{2} V^2 + \frac{1}{3} D_2 V^3 + \frac{1}{4} D_3 V^4 + \frac{1}{2} a^2 \delta_2^{-1/2} D_1 V V_{ZZ} \right).
\end{aligned} \tag{5.1}$$



Without loss of generality, we take the length of the cylinder to be 1 (then  $a = a/1$  can be regarded as the radius-length ratio) and the total potential energy is then given by

$$\Omega = \pi a^2 \int_0^1 \bar{\Psi} dZ - T \int_0^1 (\delta_2 - 1 + V) dZ = \pi a^2 \int_0^1 (\bar{\Psi} - \gamma(\delta_2 - 1 + V)) dZ. \quad (5.2)$$

By using the variational principle for this functional, we find that the Euler-Lagrange equation is exactly same as (4.12). This shows that the ANFE obeys the variational principle for energy.

The expression of the total potential energy (5.2) itself is very important. When there are multiple solutions, the smallest energy criterion can be used to judge the preferred solution (configuration).

For convenience, we set  $\bar{V} = V + \delta_2$  which is the axial stretch. Then (4.12) can be rewritten as

$$\bar{V} - \delta_2 + D_2(\bar{V} - \delta_2)^2 + D_3(\bar{V} - \delta_2)^3 + a^2 \delta_2^{-1/2} D_1 \bar{V}_{ZZ} = \frac{\gamma - D_0}{E_T}. \quad (5.3)$$

This is the ANFE governing the axial stretch in a deformation state near the homogeneous deformation with the axial stretch  $\delta_2$ .

**6. Analytical solutions for localizations at near-critical loads.** As well-known, the localization phenomenon usually takes place when the stress is close to the load maximum.

Now we conduct a detailed analysis on the ANFE (5.3) together with proper end conditions when  $\gamma$  varies near the peak value (correspondingly, the axial stretch is in the neighborhood of  $\delta_2^* = 2.04767$ ). For that purpose, we choose  $\delta_2 = 2.0$ , then from (4.11) the constant term and coefficients of equation (5.3) can be calculated and their values are:  $E_T = 0.0107233$ ,  $D_0 = 0.5821068$ ,  $D_1 = -0.1749928$ ,  $D_2 = -11.303301$ ,  $D_3 = 11.995243$ . We impose the free end conditions at  $Z = 0$  and  $Z = 1$ , i.e.

$$\bar{V}_Z = 0 \text{ at } Z = 0, 1, \quad (6.1)$$

which are sometimes called natural boundary conditions and have been used by many authors (see [22, 23]). From (5.3), we can see that the asymptotic engineering stress-stretch response (up to a third-order material nonlinearity) for a homogeneous deformation should be given by

$$\gamma = D_0 + E_T \left( \bar{V} - \delta_2 + D_2 (\bar{V} - \delta_2)^2 + D_3 (\bar{V} - \delta_2)^3 \right). \quad (6.2)$$

By varying  $\gamma$  or  $\bar{V}$ , we can get the asymptotic curve, which is shown in Figure 6.1 (a) (the dashed curve). One can see that, around the expansion point  $\delta_2 = 2.0$  this asymptotic response captures well the behavior of the homogeneous stress-stretch curve obtained directly from the strain energy function of the Blatz-Ko material. This gives some support to our approximation.

In order to conduct the phase-plane analysis to calculate the analytical solutions, we rewrite the ANFE (5.3) as a first-order system:

$$\bar{V}_Z = y, \quad y_Z = \frac{\bar{V} - \delta_2 + D_2 (\bar{V} - \delta_2)^2 + D_3 (\bar{V} - \delta_2)^3 + \frac{D_0 - \gamma}{E_T}}{-a^2 \delta_2^{-1/2} D_1}. \quad (6.3)$$

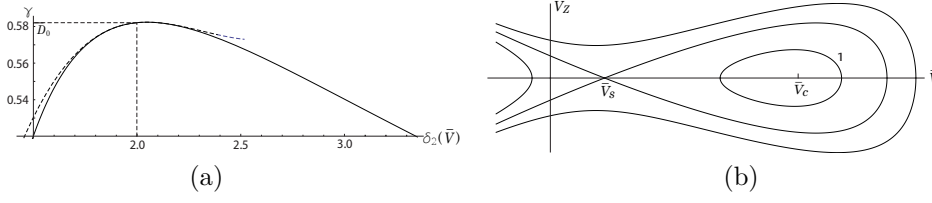


FIG. 6.1. (a) The asymptotic stress-stretch curve (the dashed curve) and the exact curve (the full line); (b) The phase plane.

And the equilibrium points of this system are given by

$$y = 0, \text{ and } \bar{V} - \delta_2 + D_2 (\bar{V} - \delta_2)^2 + D_3 (\bar{V} - \delta_2)^3 = \frac{\gamma - D_0}{E_T}. \quad (6.4)$$

One can see that the phase plane has a saddle point and a center point as  $\gamma$  varies near the peak, which is shown in Figure 6.1 (b). In this figure,  $(\bar{V}_s, 0)$  and  $(\bar{V}_c, 0)$  are a saddle point and a center point, respectively. There are three solutions for the same stress, two of them are the constant solutions, i.e.  $\bar{V}_s$  and  $\bar{V}_c$ , and the third type is the nontrivial solution, which is represented by a certain closed orbit (cf. curve 1 in Figure 6.1 (b)), as it can contact the  $\bar{V}$ -axis at least twice (so  $\bar{V}_Z = 0$  at  $Z = 0, 1$  can be satisfied). To deduce the solution expression, we integrate (5.3) once to obtain

$$H + \frac{D_0 - \gamma}{E_T} (\bar{V} - \delta_2) + \frac{1}{2} (\bar{V} - \delta_2)^2 + \frac{1}{3} D_2 (\bar{V} - \delta_2)^3 + \frac{1}{4} D_3 (\bar{V} - \delta_2)^4 + \frac{1}{2} a^2 \delta_2^{-1/2} D_1 \bar{V}_Z^2 = 0, \quad (6.5)$$

where  $H$  is an integration constant.

From the phase-plane analysis, we know that the closed orbits corresponding to some special values of  $H$  such that

$$H + \frac{D_0 - \gamma}{E_T} (\bar{V} - \delta_2) + \frac{1}{2} (\bar{V} - \delta_2)^2 + \frac{1}{3} D_2 (\bar{V} - \delta_2)^3 + \frac{1}{4} D_3 (\bar{V} - \delta_2)^4 = 0 \quad (6.6)$$

has four real roots  $g_0 \leq g_1 \leq g_2 \leq g_3$ , and  $g_1$  and  $g_2$  are the intersection points of the closed orbits and the  $\bar{V}$ -axis. Then from (6.5), we have

$$\bar{V}_Z = \pm \frac{\delta_2^{1/4}}{a} \sqrt{\frac{D_3}{-2D_1}} \sqrt{(\bar{V} - g_0)(\bar{V} - g_1)(\bar{V} - g_2)(\bar{V} - g_3)}. \quad (6.7)$$

It should be noted that under the free end boundary conditions, for a closed orbit to represent a solution, we must have  $\bar{V}|_{Z=0} = g_1$  or  $g_2$ . Here we only consider the case  $\bar{V}|_{Z=0} = g_1$ , since the solution for the other case is a simple translation of this solution ((6.3) is invariant for the transformation  $Z = 1/2 - Z$ ). From (6.7), by applying a formula in Byrd and Friedman [24] to the integral, we obtain

$$Z = \mathcal{G} a F(\phi, \chi), \quad (6.8)$$

where  $F(\phi, \chi)$  is the incomplete elliptic integral of the first kind, and

$$\mathcal{G} = \frac{2\delta_2^{-1/4} \sqrt{-2D_1}}{\sqrt{(g_3 - g_1)(g_2 - g_0)D_3}}, \quad \chi = \sqrt{\frac{(g_2 - g_1)(g_3 - g_0)}{(g_3 - g_1)(g_2 - g_0)}}, \quad \phi = \arcsin \sqrt{\frac{(g_2 - g_0)(\bar{V} - g_1)}{(g_2 - g_1)(\bar{V} - g_0)}}. \quad (6.9)$$

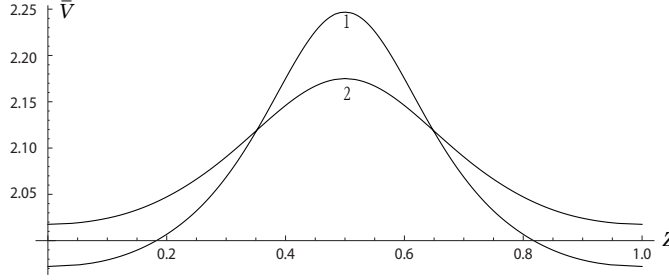


FIG. 6.2.  $\bar{V} - Z$  plot for  $a = 0.40$ . Curve 1, 2 respectively for  $\gamma = 0.5812$  and  $\gamma = 0.5819$ .

By using the Jacobian elliptic function, from (6.8), we can further obtain

$$\bar{V} = \frac{g_1 - \frac{g_2 - g_1}{g_2 - g_0} g_0 \operatorname{sn}^2\left(\frac{Z}{Ga}, \chi\right)}{1 - \frac{g_2 - g_1}{g_2 - g_0} \operatorname{sn}^2\left(\frac{Z}{Ga}, \chi\right)}. \quad (6.10)$$

We focus on the one-period solutions (orbits going around only once). Then by further using the boundary condition  $\bar{V}|_{Z=1} = g_1$ , we can determine  $H$ . In fact, from the symmetry of the closed orbit, one can see that  $\bar{V}|_{Z=1/2} = g_2$ , i.e. (see (6.8))

$$\frac{1}{2} = \mathcal{G}aF\left(\frac{\pi}{2}, \chi\right) = \mathcal{G}aK(\chi), \quad (6.11)$$

where  $K(\cdot)$  is the complete elliptic integral of the first kind. For a given  $\gamma$  near the critical load,  $H$ , and thus  $g_i$  ( $0 \leq i \leq 3$ ) can be determined uniquely by (6.11). Then, the analytical solution for  $0 \leq Z \leq 1/2$  is provided by (6.10).

**Remark:** Whether (6.11) has a solution for  $H$  determines whether there exists a nontrivial (non-constant) solution. Then, the maximum value of  $\gamma$  for which (6.11) has a solution for  $H$  is the critical load for bifurcation in a force-controlled problem. It should be noted that this load  $\gamma_0$  depends on  $a$ . For  $a = 0.40, 0.35, 0.30$ , we find that  $\gamma_0 = 0.58221, 0.58228, 0.58235$ , respectively (cf. Figure 8.5). Since the critical load is determined by this nonlinear relation (which arises from the nonlinear equation (6.7)), it appears that a linearized theory (i.e. small-on-large stability analysis) cannot determine this load. When  $a$  tends to zero (corresponding to an infinitely-long cylinder), we find that  $\gamma_0 = 0.5824$ , the maximum load in Figure 2.2.

In Figure 6.2, we have plotted the one-period solution curves for two different values of the engineering stress. Here we take  $a = 0.40$ . This value is not too large, since for  $\delta_2 = 2.0$ ,  $\nu = \delta_1^2 a^2 / \delta_2^2 l^2 \approx 0.028$  is small enough for the asymptotic method.

In this figure, we can see that there is a sharp-change region in the middle of the slender cylinder, which represents the localization and stress concentration. Moreover, the tip is sharper for a smaller engineering stress value.

**Remark:** One can also do a near-critical analysis by making the special choice  $\gamma = D_0$ . For  $\delta_2$  near  $\delta_2^*$ , to leading order Eq. (4.12) can then be replaced by

$$-a^2 \delta_2^{-1/2} V_{ZZ} = \hat{D}_1(\delta_2 - \delta_2^*)V + \hat{D}_2 V^2, \quad (6.12)$$

where  $\hat{D}_1$  is the derivative of  $D_1^{-1}$  evaluated at  $\delta_2^*$  and  $\hat{D}_2 = D_1^{-1} D_2|_{\delta_2=\delta_2^*}$ . One can then solve this slightly simpler equation to get the localized solutions. However, for the analysis in section 7 we need to allow  $\gamma$  to vary, so in this section we do not work

with the above equation. Also, it appears that (6.4) can give a better result for the position of the center point in the phase plane when  $\gamma$  is moderately away from the load maximum.

**7. Analytical solutions for large localizations.** For the Blatz-Ko material, a model describing large deformations, the stretch range of the localization may be very large. The asymptotic curve, and thus the corresponding phase plane and solutions in the previous section only make sense for the axial stretch in a small neighborhood of the expansion point. Therefore the results obtained there could not be used to describe large localizations.

To capture large localizations, we borrow the idea of using a spline to approximate a function in a large variable interval. One can divide this interval into many small neighborhoods and then in each of them one can use a polynomial to approximate this function. By further imposing proper smoothness requirements at the joint points of these neighborhoods a spline of polynomials can approximate this function well.

For the present problem, suppose that the axial stretch varies in a large interval. We choose a group of points in this interval and let the adjacent points be close enough to each other. We take the joint small neighborhoods around these points. Although each neighborhood covers a small stretch interval, the union of these neighborhoods covers the whole interval. We can do the expansion at each value of  $\delta_2$  of these points. According to the previous section, one can obtain the solution valid in the corresponding small neighborhood. The solution for a large localization can be obtained if we join these solutions (each valid in a small neighborhood) together. We remark that such a spline approximation is done in a stretch interval, not a variable interval.

To summarize, the present methodology contains the following steps: 1. Choose points in a suitable stretch interval and construct a small neighborhood for each point. 2. In each neighborhood, find the solution and join together these solutions by smoothness requirements. 3. Use boundary conditions to determine the constants appeared in the solutions. Now, we describe these steps below.

We expand the stress (cf. (2.10)) at a group of points whose  $\delta_2$  values are chosen as follows:

$$\delta_2^{(j)} = \delta_2^{(1)} + (j-1)h, \quad 1 \leq j \leq j_h, \quad (7.1)$$

where  $\delta_2^{(1)}$  is the first expansion point, and  $h$  is the step-length and  $j_h$  is the number of points. Depending on the range of the axial stretch of the localization solutions, one can make specific choices for  $\delta_2^{(1)}$ ,  $h$  and  $j_h$ . Here, we choose  $\delta_2^{(1)} = 1.7$ ,  $h = 0.05$  and  $j_h = 30$ , in order to construct the localization solutions with the axial stretch value inside the large interval (1.67, 3.17). We point out that we do not need to know the stretch interval  $[V_{\min}, V_{\max}]$  of a solution beforehand, instead we only need  $[V_{\min}, V_{\max}] \in (1.67, 3.17)$ .

The ANFE for expansion at  $\delta_2^{(j)}$  (cf. (5.3)) is

$$\bar{V} - \delta_2^{(j)} + D_2^{(j)} \left( \bar{V} - \delta_2^{(j)} \right)^2 + D_3^{(j)} \left( \bar{V} - \delta_2^{(j)} \right)^3 + a^2 \left( \delta_2^{(j)} \right)^{-1/2} D_1^{(j)} \bar{V}_{ZZ} = \frac{\gamma - D_0^{(j)}}{E_T^{(j)}}, \quad (7.2)$$

where

$$E_T^{(j)} = E_T \left( \delta_2^{(j)} \right), \quad D_i^{(j)} = D_i \left( \delta_2^{(j)} \right), \quad i = 0, 1, 2, 3, \quad (7.3)$$

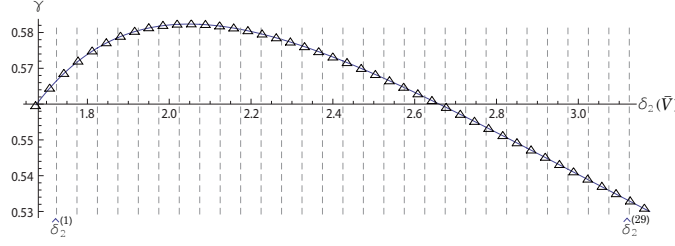


FIG. 7.1. The asymptotic engineering stress-stretch curve (full line) and the exact curve ( $-\Delta-$ )

are the coefficients dependent on  $\delta_2^{(j)}$ . From the ANFE (7.2), one can see that the asymptotic engineering stress-stretch response near  $\delta_2^{(j)}$  for a homogeneous deformation should be given by

$$\gamma = D_0^{(j)} + E_T^{(j)} \left( \bar{V} - \delta_2^{(j)} + D_2^{(j)} \left( \bar{V} - \delta_2^{(j)} \right)^2 + D_3^{(j)} \left( \bar{V} - \delta_2^{(j)} \right)^3 \right). \quad (7.4)$$

We shall use the above expression to construct a small neighborhood  $(\hat{\delta}_2^{(j-1)}, \hat{\delta}_2^{(j)})$  containing  $\delta_2^{(j)}$ . More specially,  $\hat{\delta}_2^{(j)}$  is determined by requiring that the  $j$ -th asymptotic curve and  $(j+1)$ -th asymptotic curve intersects at  $\bar{V} = \hat{\delta}_2^{(j)}$ , i.e.,

$$\begin{aligned} D_0^{(j)} + E_T^{(j)} \left( \hat{\delta}_2^{(j)} - \delta_2^{(j)} + D_2^{(j)} \left( \hat{\delta}_2^{(j)} - \delta_2^{(j)} \right)^2 + D_3^{(j)} \left( \hat{\delta}_2^{(j)} - \delta_2^{(j)} \right)^3 \right) = \\ D_0^{(j+1)} + E_T^{(j+1)} \left( \hat{\delta}_2^{(j)} - \delta_2^{(j+1)} + D_2^{(j+1)} \left( \hat{\delta}_2^{(j)} - \delta_2^{(j+1)} \right)^2 + D_3^{(j+1)} \left( \hat{\delta}_2^{(j)} - \delta_2^{(j+1)} \right)^3 \right). \end{aligned} \quad (7.5)$$

All  $\hat{\delta}_2^{(j)}$  ( $j = 1, \dots, j_h - 1$ ) can be determined from (7.5). Then, by letting  $j = 1, \dots, j_h - 1$  in (7.4) we can obtain an asymptotic engineering stress-stretch curve for  $\bar{V}$  from 1.67 to 3.17, which is plotted in Figure 7.1. It can be seen that it agrees with the exact curve very well. Actually, (7.4) is a spline approximation of the engineering stress-stretch curve.

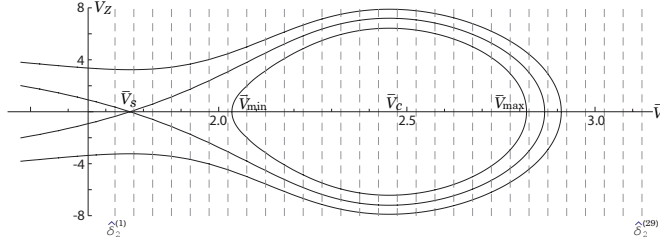
In order to construct the solutions, we now conduct a phase-plane analysis with the engineering stress as the bifurcation parameter. For  $\bar{V}$  in  $(\hat{\delta}_2^{(j-1)}, \hat{\delta}_2^{(j)})$ , we can rewrite (7.2) as a first-order system by

$$\bar{V}_Z = y, \quad y_Z = \frac{\bar{V} - \delta_2^{(j)} + D_2^{(j)} \left( \bar{V} - \delta_2^{(j)} \right)^2 + D_3^{(j)} \left( \bar{V} - \delta_2^{(j)} \right)^3 + \frac{D_0^{(j)} - \gamma}{E_T^{(j)}}}{-a^2 \left( \delta_2^{(j)} \right)^{-1/2} D_1^{(j)}}. \quad (7.6)$$

One can see that this system governs the part of the phase plane restricted in the small neighborhood  $\bar{V} \in (\hat{\delta}_2^{(j-1)}, \hat{\delta}_2^{(j)})$ . Joining all parts together ( $j = 1, \dots, j_h$ ), we can obtain the phase plane for a given  $\gamma$ . For  $\gamma = 0.5707$ , the phase plane is shown in Figure 7.2.

Now we study the nontrivial solutions. Eq. (7.2) can be integrated once to give

$$\begin{aligned} H^{(j)} + \frac{D_0^{(j)} - \gamma}{E_T^{(j)}} \left( \bar{V} - \delta_2^{(j)} \right) + \frac{1}{2} \left( \bar{V} - \delta_2^{(j)} \right)^2 + \frac{1}{3} D_2^{(j)} \left( \bar{V} - \delta_2^{(j)} \right)^3 + \\ \frac{1}{4} D_3^{(j)} \left( \bar{V} - \delta_2^{(j)} \right)^4 + \frac{1}{2} a^2 \left( \delta_2^{(j)} \right)^{-1/2} D_1^{(j)} \bar{V}_Z^2 = 0, \end{aligned} \quad (7.7)$$

FIG. 7.2. The phase plane for  $\gamma = 0.5707$ .

where  $H^{(j)}$  are the integration constants. To guarantee the corresponding orbits in the adjacent pieces of the phase plane joined continuously, we impose that

$$\lim_{\bar{V} \rightarrow \hat{\delta}_2^{(j)-}} \bar{V}_Z = \lim_{\bar{V} \rightarrow \hat{\delta}_2^{(j)+} } \bar{V}_Z. \quad (7.8)$$

Taking the above left and right limits in equations (7.7), we can see that these integration constants should satisfy

$$\frac{H^{(j)} + \frac{D_0^{(j)} - \gamma}{E_T^{(j)}} (\hat{\delta}_2^{(j)} - \delta_2^{(j)}) + \frac{1}{2} (\hat{\delta}_2^{(j)} - \delta_2^{(j)})^2 + \frac{1}{3} D_2^{(j)} (\hat{\delta}_2^{(j)} - \delta_2^{(j)})^3 + \frac{1}{4} D_3^{(j)} (\hat{\delta}_2^{(j)} - \delta_2^{(j)})^4}{(\delta_2^{(j)})^{-1/2} D_1^{(j)}} = \frac{H^{(j+1)} + \frac{D_0^{(j+1)} - \gamma}{E_T^{(j+1)}} (\hat{\delta}_2^{(j)} - \delta_2^{(j+1)}) + \frac{1}{2} (\hat{\delta}_2^{(j)} - \delta_2^{(j+1)})^2 + \frac{1}{3} D_2^{(j+1)} (\hat{\delta}_2^{(j)} - \delta_2^{(j+1)})^3 + \frac{1}{4} D_3^{(j+1)} (\hat{\delta}_2^{(j)} - \delta_2^{(j+1)})^4}{(\delta_2^{(j+1)})^{-1/2} D_1^{(j+1)}}, \quad 1 \leq j \leq j_h - 1. \quad (7.9)$$

For an orbit in the phase plane, one can see that under the above conditions, its corresponding solution  $\bar{V}$  and its derivative  $\bar{V}_Z$  are both continuous at the lines  $\bar{V} = \hat{\delta}_2^{(j)}$ . Obviously equations (7.9) have only one free unknown, and  $H^{(j)}$  ( $1 \leq j \leq j_h$ ) can be considered as functions of  $H^{(m)}$  for a chosen  $m$  ( $1 \leq m \leq j_h$ ). Therefore every orbit in Figure 7.2 is uniquely determined by the integration constant  $H^{(m)}$ .

With the natural boundary condition (6.1), the nontrivial solutions are represented by the closed orbits. For a given  $\gamma$ , there are infinitely-many closed orbits in a phase plane. Suppose that a closed orbit has the axial stretch value  $\bar{V}$  inside  $(\hat{\delta}_2^{(k_1-1)}, \hat{\delta}_2^{(k_2)}]$  for some integers  $1 \leq k_1 \leq k_2 \leq j_h$  with the minimum and maximum values  $\bar{V}_{\min}$  and  $\bar{V}_{\max}$  respectively. From (7.7) we can write the expression of  $\bar{V}_Z$  as a piecewise continuous function of  $\bar{V}$  for this closed orbit:

$$\bar{V}_Z = \begin{cases} \pm \frac{(\delta_2^{(k_1)})^{1/4}}{a} \sqrt{M(\bar{V}, k_1)}, & \bar{V}_{\min} < \bar{V} \leq \hat{\delta}_2^{(k_1)}, \\ \pm \frac{(\delta_2^{(j)})^{1/4}}{a} \sqrt{M(\bar{V}, j)}, & \hat{\delta}_2^{(j-1)} < \bar{V} \leq \hat{\delta}_2^{(j)}, \quad k_1 + 1 \leq j \leq k_2 - 1, \\ \pm \frac{(\delta_2^{(k_2)})^{1/4}}{a} \sqrt{M(\bar{V}, k_2)}, & \hat{\delta}_2^{(k_2-1)} < \bar{V} \leq \bar{V}_{\max}, \end{cases} \quad (7.10)$$

where

$$M(\bar{V}, j) = -\frac{2H^{(j)}}{D_1^{(j)}} - \frac{2(D_0^{(j)} - \gamma)}{E_T^{(j)} D_1^{(j)}} (\bar{V} - \delta_2^{(j)}) - (\bar{V} - \delta_2^{(j)})^2 - \frac{2D_2^{(j)}}{3D_1^{(j)}} (\bar{V} - \delta_2^{(j)})^3 - \frac{D_3^{(j)}}{2D_1^{(j)}} (\bar{V} - \delta_2^{(j)})^4, \quad k_1 \leq j \leq k_2. \quad (7.11)$$

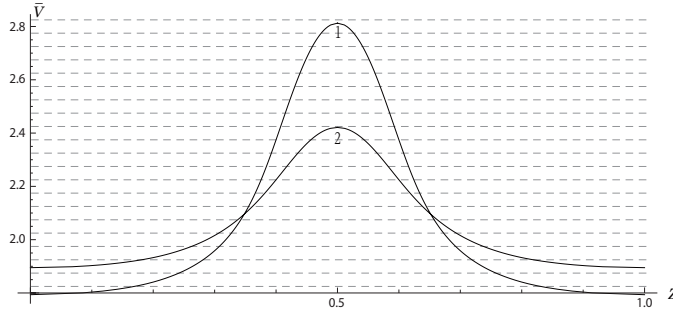


FIG. 7.3.  $\bar{V} - Z$  plot. Curve 1, 2 respectively for  $\gamma = 0.5717$  and  $\gamma = 0.5787$ .

**Remark:** If  $k_2 = k_1$ , there is only one piece, and if  $k_2 = k_1 + 1$  there are only two pieces. Here, we omit the expressions for these two cases.

In order that the closed orbit described by (7.10) is the solution, the boundary condition (6.1) has to be satisfied. Here, we focus on the one-period solution. Without loss of generality, we also take the left intersection point between the close orbit and the  $\bar{V}$ -axis as the initial point of the solution, i.e.  $\bar{V}|_{Z=0} = \bar{V}_{\min}$ . Then, for the one-period solution the  $Z$ -interval for  $\bar{V}$  from the minimum to the maximum should be  $1/2$ . From (7.10), we have

$$\frac{1}{2} = \mathcal{F}\left(k_1, \bar{V}_{\min}, \hat{\delta}_2^{(k_1)}\right) + \sum_{j=k_1+1}^{k_2-1} \mathcal{F}\left(j, \hat{\delta}_2^{(j-1)}, \hat{\delta}_2^{(j)}\right) + \mathcal{F}\left(k_2, \hat{\delta}_2^{(k_2-1)}, \bar{V}_{\max}\right), \quad (7.12)$$

where  $\mathcal{F}$  is an integral defined by

$$\mathcal{F}(j, \alpha, \beta) = a \left(\hat{\delta}_2^{(j)}\right)^{-1/4} \int_{\alpha}^{\beta} \frac{d\bar{V}}{\sqrt{M(\bar{V}, j)}}. \quad (7.13)$$

Consequently, integrating (7.10) once, we obtain the expressions of the one-period solutions (the first-half period):

$$Z = \begin{cases} \mathcal{F}\left(k_1, \bar{V}_{\min}, \bar{V}\right), & 0 \leq Z \leq Z^{(k_1)}, \\ \mathcal{F}\left(k_1, \bar{V}_{\min}, \hat{\delta}_2^{(k_1)}\right) + \sum_{j=k_1+1}^{k-1} \mathcal{F}\left(j, \hat{\delta}_2^{(j-1)}, \hat{\delta}_2^{(j)}\right) + \mathcal{F}\left(k, \hat{\delta}_2^{(k-1)}, \bar{V}\right), & Z^{(k-1)} < Z \leq Z^{(k)}, \\ \mathcal{F}\left(k_1, \bar{V}_{\min}, \hat{\delta}_2^{(k_1)}\right) + \sum_{j=k_1+1}^{k_2-1} \mathcal{F}\left(j, \hat{\delta}_2^{(j-1)}, \hat{\delta}_2^{(j)}\right) + \mathcal{F}\left(k_2, \hat{\delta}_2^{(k_2-1)}, \bar{V}\right), & k_1 + 1 \leq k \leq k_2 - 1, \\ \mathcal{F}\left(k_1, \bar{V}_{\min}, \hat{\delta}_2^{(k_1)}\right) + \sum_{j=k_1+1}^{k_2-1} \mathcal{F}\left(j, \hat{\delta}_2^{(j-1)}, \hat{\delta}_2^{(j)}\right) + \mathcal{F}\left(k_2, \hat{\delta}_2^{(k_2-1)}, \bar{V}\right), & Z^{(k_2-1)} < Z \leq \frac{1}{2}, \end{cases} \quad (7.14)$$

where  $Z^{(k)}$  satisfies  $\bar{V}(Z^{(k)}) = \hat{\delta}_2^{(k)}$ . Once  $k_1$ ,  $k_2$ ,  $\bar{V}_{\min}$  and  $\bar{V}_{\max}$  are found, (7.14) provides the solution.

We point out that depending on the roots of  $M(\bar{V}, j) = 0$  the integral in (7.13) can be represented by different elliptic integrals (the detailed expressions are omitted due to space limit). This is why we call the solutions to be elliptic-spline solutions.

Now we describe the procedure for determining  $k_1$ ,  $k_2$ ,  $\bar{V}_{\min}$  and  $\bar{V}_{\max}$ .

For a given  $\gamma$ , one can find from (7.4) the saddle point  $(\bar{V}_s, 0)$  and center point  $(\bar{V}_c, 0)$ , and we have  $\bar{V}_s < \bar{V}_{\min} < \bar{V}_c$  and  $\bar{V}_{\max} > \bar{V}_c$  (see Figure 7.2). Then, we calculate the  $Z$ -interval of the closed orbit from the minimum value  $\bar{V}_{\min}$  to the maximum value  $\bar{V}_{\max}$  for a chosen  $\bar{V}_{\min}$  as follows. Since  $\hat{\delta}_2^{(k_1-1)} < \bar{V}_{\min} \leq \hat{\delta}_2^{(k_1)}$ ,  $k_1$

can be found, and  $H^{(k_1)}$  can be obtained from (7.7) by setting  $\bar{V} = \bar{V}_{\min}$  and  $\bar{V}_Z = 0$ . Then,  $H^{(j)}$  ( $k_1 + 1, k_1 + 2, \dots$ ) can be calculated from (7.9). We can determine the number  $k_2$  from (7.11) by requiring:

$$M(\hat{\delta}_2^{(k_2-1)}, k_2 - 1) > 0, \quad M(\hat{\delta}_2^{(k_2)}, k_2) \leq 0, \quad (7.15)$$

since for the closed orbit  $\bar{V}_Z$  (cf. (7.10)) is real for  $\bar{V}_{\min} \leq \bar{V} \leq \bar{V}_{\max}$  and is undefined for  $\bar{V}_{\max} < \bar{V} \leq \hat{\delta}_2^{(k_2)}$  if  $\hat{\delta}_2^{(k_2)} > \bar{V}_{\max}$  (for the case  $\hat{\delta}_2^{(k_2)} = \bar{V}_{\max}$ , the equality in (7.15)<sub>2</sub> holds). Also, the maximum value, which should satisfy  $\hat{\delta}_2^{(k_2-1)} < \bar{V}_{\max} \leq \hat{\delta}_2^{(k_2)}$ , can be determined uniquely from

$$M(\bar{V}_{\max}, k_2) = 0. \quad (7.16)$$

Then, taking an integration in (7.10), we can find the  $Z$ -interval  $S(\bar{V}_{\min})$ . If  $S(\bar{V}_{\min}) = 1/2$  (i.e., (7.12) is satisfied), then  $k_1, k_2, \bar{V}_{\min}$  and  $\bar{V}_{\max}$  for the one-period solution have been determined as above. If  $S(\bar{V}_{\min}) \neq 1/2$ , we just vary  $\bar{V}_{\min}$  in the interval  $(\bar{V}_s, \bar{V}_c)$  until a  $\bar{V}_{\min}$  is found such that  $S(\bar{V}_{\min}) = 1/2$ .

For  $a = 0.40$ , the plots of the one-period solutions for  $\gamma = 0.5717$  ( $k_1 = 3, k_2 = 23, \bar{V}_{\min} = 1.7935, \bar{V}_{\max} = 2.8125$ ) and  $\gamma = 0.5787$  ( $k_1 = 5, k_2 = 15, \bar{V}_{\min} = 1.8949, \bar{V}_{\max} = 2.4212$ ) are shown in Figure 7.3. We point out that this value of  $a$  is not too large, since we only need  $\nu_{\min} = (\delta_1^{(j)} a)^2 / (\delta_2^{(j)} l)^2 = (\delta_1^{(1)} a)^2 / (\delta_2^{(1)} l)^2$  to be small enough. In fact, when  $a = 0.40$ ,  $\nu_{\min} = 0.042$  is in the allowable range.

**8. Large localizations in a displacement-controlled problem.** The solutions obtained in the above section are for a given  $\gamma$ . We now consider a displacement-controlled problem such that the total elongation  $\Delta - 1$  is given, where

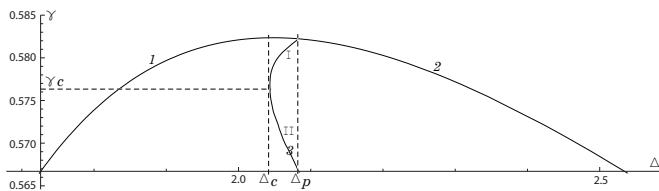
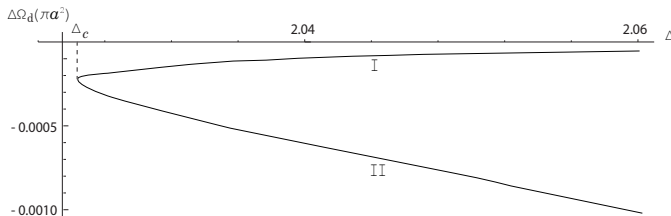
$$\Delta = \int_0^1 \bar{V} dZ = 2 \int_0^{\frac{1}{2}} \bar{V} dZ = 2 \sum_{j=k_1}^{k_2} \int_{Z^{(j-1)}}^{Z^{(j)}} \bar{V} dZ, \quad (8.1)$$

where we define  $Z^{(k_1-1)} = 0$  and  $Z^{(k_2)} = 1/2$ . The governing equation is still (7.2), but now  $\gamma$  is an unknown parameter. However, if for a given  $\Delta$ , we can find the corresponding  $\gamma$ , then we can obtain the solutions by the steps given in the previous section. The difficulty is that for a given  $\Delta$ , there may be multiple values for  $\gamma$ . In the following, we also only consider the one-period solutions and choose  $a = 0.40$ .

In Figure 8.1, we plot the  $\gamma - \Delta$  curves for the constant solutions and the one-period solution obtained in section 7. In this figure, segment 1 and segment 2 correspond to the constant solutions  $\bar{V}_s$  and  $\bar{V}_c$  respectively, and segment 3 corresponds to the one-period solution. It can be seen that there exist multiple solutions if  $\Delta$  takes a value equal to or greater than  $\Delta_c$ . In fact, as  $\Delta$  increases, there are bifurcations from one solution to two solutions (at  $\Delta = \Delta_c$ ), to three solutions ( $\Delta_c < \Delta < \Delta_p$ ), and to two solutions ( $\Delta \geq \Delta_p$ ). For a given  $\Delta = \Delta_0$ , we can draw the vertical line  $\Delta = \Delta_0$  in Figure 8.1 to find the stress values at the intersection points with the  $\gamma - \Delta$  curves. Once the stress values are obtained, the solutions can be obtained from (7.12) and (7.14).

**Remark:** For a displacement-controlled problem, the bifurcation point  $\Delta = \Delta_c$  is only found when the post-bifurcation solutions of the boundary-value problem are obtained. This indicates that a small-on-large stability analysis cannot capture this bifurcation point. A weakly nonlinear theory may not capture it either, since the axial stretch value varies in a large interval at this point and the state is not near a homogeneous one.



FIG. 8.1. The  $\gamma - \Delta$  plot for  $a = 0.40$ .FIG. 8.2. Differences of the total stored energies between solutions I, II and the constant solutions for  $\Delta_c < \Delta < \Delta_*$  ( $a = 0.40$ ).

We now find the preferred solution when  $\Delta \geq \Delta_c$ . But, first we examine the strong ellipticity condition for the solutions obtained. For the Blatz-Ko material, Knowles & Sternberg [25] showed that the strong ellipticity never fails if and only if

$$2 - \sqrt{3} < \frac{\lambda_i}{\lambda_j} < 2 + \sqrt{3} \quad (i \neq j), \quad (8.2)$$

where  $\lambda_i, \lambda_j (i, j = 1, 2, 3)$  are the principal stretches. As the solutions for a given  $\gamma$  have been obtained, we can verify the condition (8.2) directly. It is interesting to note that for the homogeneous deformation (8.2) is satisfied if  $\delta_2 < 2.86$ , which is significantly larger than  $\delta_2^* = 2.04767$ , the stretch value at the maximum load. And we find that, for one-period solutions (8.2) is satisfied when  $\gamma > 0.5706$ . The corresponding  $\Delta$  of the one-period solution for  $\gamma = 0.5706$  is  $\Delta_* = 2.06$ . That is to say, when  $\Delta \geq \Delta_*$  the corresponding solutions are unstable, so we only consider the preferred solution when  $\Delta_c \leq \Delta < \Delta_*$ .

For this purpose we calculate the total potential energies of all the possible solutions for  $\Delta_c \leq \Delta < \Delta_*$ . By using (5.1), one can calculate the potential energy values of the nontrivial solutions. And the total potential energy values for constant solutions can be easily calculated from the strain energy function directly.

From Figure 8.1, one can see that when  $\Delta$  is between  $\Delta_c$  and  $\Delta_*$ , there are three possible solutions, two of them are nontrivial solutions labeled by I, II from top to bottom, respectively. We plot in Figure 8.2 the differences (denoted by  $\Delta \Omega_d$ ) of the total potential energies between the two one-period solutions I, II and the constant solution for  $\Delta_c \leq \Delta < \Delta_*$ .

If we take the solution with the smallest energy value as the preferred one, then from Figure 8.2, we can see that for  $\Delta < \Delta_c$  the constant solution is the preferred one, and for  $\Delta_c \leq \Delta < \Delta_*$  the one-period solution corresponding to the least stress is the preferred one. The structure response curve ( $\gamma - \Delta$  curve) corresponding to the preferred solution is shown in Figure 8.3. It is worth noting that a snap-through takes place at  $\Delta = \Delta_c$  (there exists a stress drop to  $\gamma_c$ ), which leads to the localization.

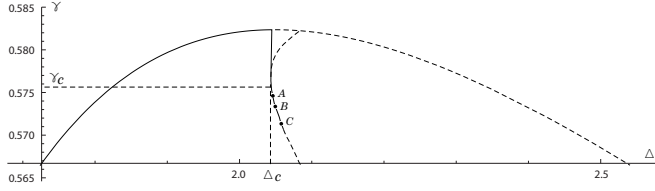


FIG. 8.3. The  $\gamma - \Delta$  curve corresponding to the preferred solution for  $a = 0.40$ .

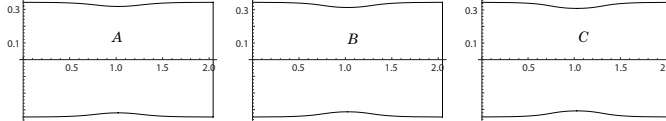


FIG. 8.4. Profiles of the cylinder at different stages.

What we have solved is a problem in a three-dimensional setting, and as a result the three-dimensional displacement field can be determined. In Figure 8.4, we draw the profiles of the cylinder at different stages corresponding to points  $A$ ,  $B$  and  $C$  in Figure 8.3 (the corresponding axial stretches are  $\Delta_A = 2.043$ ,  $\Delta_B = 2.046$ ,  $\Delta_C = 2.056$ ).

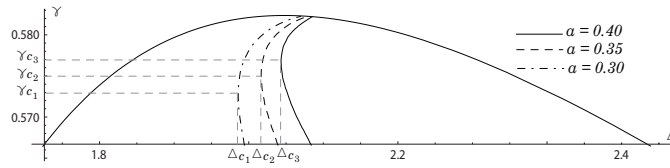
Figure 8.4 also shows that the middle part of the cylinder becomes thinner than the two ends as we pull the slender cylinder. The middle part becomes thinner as the engineering stress decreases. We note that, when  $\Delta_C = 2.056$  (the total stretch), the largest axial stretch value appeared at  $Z = 1/2$  is 2.8125, which is significantly larger than the total stretch.

From the expression of the nontrivial solutions (7.14) and (7.13), we can see that the radius of the cylinder  $a$  (can also be considered as the radius-length ratio as we have already chosen the length of the cylinder to be 1) has an important influence on the properties of the nontrivial solutions.

By the same steps in the previous sections, we can get the relations between the total stretch and the engineering stress corresponding to some different values of  $a$ , which are shown in Figure 8.5. From this figure, we observe that there is a snap-back for a relatively small value of  $a$ . And we can also obtain the critical point  $(\Delta_c, \gamma_c)$  in Figure 8.5 for different  $a$ :  $(\Delta_{c1}, \gamma_{c1}) = (1.985, 0.5726)$  for  $a = 0.30$ ,  $(\Delta_{c2}, \gamma_{c2}) = (2.017, 0.5757)$  for  $a = 0.35$  and  $(\Delta_{c3}, \gamma_{c3}) = (2.043, 0.5765)$  for  $a = 0.40$ . We can see that there is no unique stress-displacement relationship in the post-peak region. And as the value of  $a$  increases the point  $(\Delta_c, \gamma_c)$  also moves up and toward right. From this result we can reach the conclusion: the thinner the specimen, the steeper the curve.

**Remark:** The behavior of large localizations for the compressible Blatz-Ko material obtained in this section seems to agree with the experimental results described in [8, 9], which found that the tangent value in the ascending part of the stress-strain curves seems to be independent of the specimen size but the post-peak response seems not only a material property but is dependent on the specimen geometry, and the post-peak response becomes steeper with increasing length of the specimen.

**9. Conclusions.** We have proposed a novel approach—within a three-dimensional framework with strong nonlinearity—to analytically tackle the large localization problem of a circular cylinder composed of a Blatz-Ko material. The asymptotic normal form equation near an arbitrary axial stretch is derived by the method of coupled

FIG. 8.5. The  $\gamma - \Delta$  curves for different  $a$ .

series-asymptotic expansions. Then the large localization problem is governed by a set of these equations for a proper group of stretch values with proper end conditions. A phase-plane analysis, which is based on a phase plane joined by small pieces cut off from their respective original phase planes, is conducted to construct the elliptic-spline solutions. The continuity of orbits in the joint phase plane guarantees that the elliptic-spline solution is  $C^1$ -continuous at the joint points. Finally, the analytical solutions obtained are successfully used to study the displacement-controlled problem and the geometrical size effect. Our results reveal that for a force-controlled problem the critical load for bifurcation, which is dependent on the radius-length ratio, is determined from a nonlinear equation. This indicates that a linearized analysis cannot capture this critical load. It is also demonstrated that for a displacement-controlled problem one needs to work in the setting of strong nonlinearity to capture the critical elongation for bifurcation. We expect that this novel approach developed here may also be used to study other instability problems with large deformations.

## REFERENCES

- [1] B. D. COLEMAN, *Necking and drawing in polymeric fibers under tension*, Arch. Rat. Mech. Anal. 83 (1983), pp. 115-137.
- [2] B. D. COLEMAN AND M. L. HODGDON, *On shear bands in ductile materials*, Arch. Rat. Mech. Anal. 90 (1985), pp. 219-247.
- [3] H.-H. DAI AND Q. S. BI, *On constructing the unique solution for the necking in a hyper-elastic rod*, J. Elasticity 82 (2006), pp. 215-241.
- [4] N. TRIANTAFYLIDIS AND E. C. AIFANTIS, *A gradient approach to localization of deformation. I. Hyperelastic materials*, J. Elasticity 16 (1986), pp. 225-237.
- [5] N. TRIANTAFYLIDIS AND S. BARDENHAGEN, *On higher order gradient continuum theories in 1-D nonlinear elasticity. Derivation from and comparison to the corresponding discrete models*, J. Elasticity 33 (1993), pp. 259-293.
- [6] E. C. AIFANTIS AND J. B. SERRIN, *Equilibrium solutions in the mechanical theory of fluid microstructures*, J. Coll. and Interfi. Sci. 96 (1983), pp. 530-547.
- [7] E. C. AIFANTIS, *On the microstructural origin of certain inelastic models*, J. Eng. Mater. Technol. 106 (1984), pp. 326-330.
- [8] D. C. JANSEN AND S. P. SHAH, *Effect of length on compressive strain softening of concrete*, J. Eng. Mech. 123 (1997), pp. 25-35.
- [9] V. S. GOPALARATNAM AND S. P. SHAH, *Softening response of plain concrete in direct tension*, J. Am. Concrete I. 82 (1985), pp. 310-323.
- [10] V. TVERGAARD, A. NEEDLEMAN AND K. K. LO, *Flow localization in the plain strain tensile test*, J. Mech. Phys. Solids 29 (1981), pp. 115-142.
- [11] A. F. BOWER, *Applied mechanics of solids*, CRC Press, 1st edition, (2009).
- [12] M. F. BEATTY, *Topics in finite elasticity: hyperelasticity of rubber, elastomers, and biological tissues-with examples*, Appl. Mech. Rev. 40 (1987), pp. 1699-1734.
- [13] Y B. FU, *Perturbation methods and nonlinear stability analysis*, Nonlinear Elasticity, Theory and Applications (London Mathematical Society Series), Cambridge Univ. Press (2001), pp. 345-391.
- [14] H.-H. DAI AND Y. HUO, *Asymptotically approximate model equations for nonlinear dispersive waves in incompressible elastic rods*, Acta. Mech. 157 (2002), pp. 97-112.
- [15] H.-H. DAI AND X. J. FAN, *Asymptotically approximate model equations for weakly nonlinear*

- long waves in compressible elastic rods and their comparisons with other simplified model equations*, Math. Mech. Solids 9 (2004), pp. 61-79.
- [16] H.-H. DAI AND Z. X. CAI, *Phase transitions in a slender cylinder composed of an incompressible elastic material. I. Asymptotic model equation*, Proc. R. Soc. Lond. Ser. A Math. Phys. Eng. Sci. 462 (2006), pp. 75-95.
- [17] H.-H. DAI AND F.-F. WANG, *Asymptotic bifurcation solutions for compressions of a clamped nonlinearly elastic rectangle: transition region and barrelling to a corner-like profile*, SIAM J. Appl. Math. 70 (2010), pp. 2673-2692.
- [18] H.-H. DAI AND F.-F. WANG, *Analytical solutions for the post-buckling states in the compression of an incompressible hyperelastic layer*, to appear in Analysis and Applications.
- [19] H.-H. DAI, Y. H. HAO AND Z. CHEN, *On constructing the analytical solutions for localizations in a slender cylinder composed of an incompressible hyperelastic material*, Inter. J. Solids Struct. 45 (2008), pp. 2613-2628.
- [20] P. J. BLATZ AND W. L. KO, *Application of finite elasticity to the deformation of rubbery materials*, Trans. Soc. Rheol. 6 (1962), pp. 223-251.
- [21] Y. B. FU AND R. W. OGDEN, *Nonlinear stability analysis of pre-stressed elastic bodies*, Continuum Mech. Thermodyn. 11 (1999), pp. 141-172.
- [22] J. L. ERICKSEN, *Equilibrium of bars*, J. Elasticity 5 (1975), pp. 191-201.
- [23] P. TONG, C. C. LAM AND Q. P. SUN, *Phase transformation of thin wires in tension*, Proceedings of the IUTAM Symposium on Mechanics of Martensitic Phase Transformation in Solids, HongKong, Kluwer Academic Publishers, Boston, 11-15 June 2001 (ed. Q. P. Sun), pp. 221-232.
- [24] P. F. BYRD AND M. D. FRIEDMAN, *Handbook of elliptic integrals for engineers and scientists*, Springer-Verlag, second ed. (1971).
- [25] J. K. KNOWLES AND E. STERNBERG, *On the ellipticity of the equations of nonlinear elastostatics for a special material*, J. Elasticity 5 (1975), pp. 341-361.